International Journal of Applied Engineering Research ISSN 0973-4562 Volume 12, Number 22 (2017) pp. 12971-12981

60 GHz Millimeter-Wave Indoor Propagation Path Loss Models

Anas Alsalman[1] and Nidal Qasem[2,*]

[1,2] Department of Electronics and Communications Engineering, Al-Ahliyya Amman University, Amman, Jordan.

**Corresponding author*
Orcid: 0000-0003-3450-9406

Abstract

The past few years, the increased demand of multimedia applications and the growth in mobile data transfer have congested the 60 GHz sub-band. Therefore, millimeter-waves (mm-waves) are used to meet the needs of users. The 60 GHz band has recently received much attention because it enables attractive gigabit-per-second wireless applications. However, this band suffers great attenuation and penetration by obstacles. Hence, it has more restrictions placed on its use. This study simulates indoor mm-wave propagation at 61.5 GHz frequency, analyses the main types of Path Loss Models (PLMs), and demonstrates the Root Mean Square (RMS) delay spread for co- and cross-polarizations. "Wireless InSite" was used to simulate the 4th floor inside the Faculty of Engineering at Al-Ahliyya Amman University in order to generate a large-scale PLM at a frequency of 61.5 GHz. The simulation used a set of three omnidirectional Transmitters (TXs), each with 3 dBi antenna gain and 25 dBm transmission power, and 26 directional Receivers (RXs), each with 8.5 dBi antenna gain, at distances ranging from 2.5 to 11.5 m for co- and cross-polarized antennas, both in Line-Of-Sight (LOS) and Non-Line-Of-Sight (NLOS) cases. The results showed that using the single-frequency Close-In (CI) reference distance PLM was the simplest solution, with fewer parameters, and ease of calculation and prediction.

Keywords: 60 GHz, Large-scale PLMs, CI, CIX, FI, RMS delay spread, Simulation, mm-wave, Indoor propagation.

INTRODUCTION

The rapid growth of personal communication devices, such as smart phones and tablets, coupled with consumer demand for ubiquitous data access, has motivated carriers to provide higher data rates and quality. Innovative technologies and new frequency bands, such as millimeter-waves (mm-waves) are needed to meet this demand [1].

The 60 GHz frequency band (frequencies of 57 to 64 GHz are available in North America and South Korea, and 59 to 66 GHz is available in Europe and Japan) has been identified by Federal Communications Commission through several administrations as being suitable for a range of short-range communications technologies, and there are indications that equipment which utilizes this band is starting to become available [2]. The considerable amount of available bandwidth in 9 GHz (from 57 to 66 GHz) could enable multi gigabit communications for cellular, office, and in-home applications as a part of a fifth generation (5G) wireless system [3-9].

The propagation characteristics of the 60 GHz band are characterized by a high level of oxygen absorption and rain attenuation. At Non-Line-Of-Sight (NLOS), the 60 GHz frequency band suffers losses in obscurity of seculars, and reflection due to the low level of diffracted signals around obstacles, such as a room corner. This strict Path Loss (PL) curbs data bandwidth and limits coverage to under 10 meters. However, it does allow a high level of frequency reuse, and, therefore, remains attractive for a variety of short-range communications applications [10-13].

Path Loss Models (PLMs) are very important tools with which to comprehend and study the attenuation of signal propagation from Transmitters (TXs) to Receivers (RXs), and they allow the design of accurate channel models for network simulations, which help in designing communications systems. The most common single-frequency PLMs are the free space Close-In (CI) reference distance, free space CI reference distance with cross-polarized discriminator (CIX), and Floating Intercept (FI) models. These models will all be studied in this paper [14].

This research provides a comprehensive study of indoor propagation at the 60 GHz frequency band using different types of antennas, polarizations, and indoor materials to generate a large-scale PLM for enhancing 5G standards at 60 GHz frequency band. Regardless, extensive indoor propagation simulations at the 60 GHz band are needed to accurately characterize and model the channel in order to design a capable indoor system at this band.

The unlicensed 60 GHz band spectrum (starting at 57.24 GHz and ending at 65.88 GHz) has been divided into four 2.16 GHz bandwidth channels. Considering the worldwide frequency allocation for unlicensed operation at the 60 GHz band, the second channel (61.5 GHz) has been selected for this study since it is commonly used in different regions and countries [15].

This paper is organized as follows: Section 2 explains large-scale PLMs. Next, Section 3 examines the simulation setup using 'Wireless InSite". Then, Section 4 discusses the investigations and demonstrates the results of PLMs for some selected scenarios using "Wireless InSite." Next, Section 5 explains the delay spread calculations and results. Finally, Section 6 concludes this paper.

LARGE-SCALE PLMS

Large-scale PLMs estimate attenuation over the distance of propagation signals and are vital for designing communications systems. Different types (deterministic, empirical, and stochastic) of large-scale PLMs exist, but measurement-based PLMs provide realistic insight into the propagation characteristics of a wireless channel [16]. Three types of PLMs have been studied in this paper: CI, CIX, and FI. The CI PLM is defined by the Path Loss Exponent (PLE), n [14, 17]:

$$PL^{CI}(f,d)[dB] = FSPL(f,d_o) + 10nlog_{10}\left(\frac{d}{d_0}\right) + X_\sigma^{CI} \quad (1)$$

$$FSPL(f,d_o) = 10log_{10}\left(\frac{4\pi d_o}{\lambda}\right)^2 \quad (2)$$

where λ is the wavelength in m, $d_o = 1$ m, and X_σ^{CI} is a zero mean Gaussian random variable with standard deviation σ^{CI} given by [14, 16]:

$$X_\sigma^{CI} = PL^{CI}(f,d)[dB] - FSPL(f,d_o)[dB] - 10nlog_{10}(d) = A - nD \quad (3)$$

$$\sigma^{CI} = \sqrt{\sum \frac{X_\sigma^{CI^2}}{N}} = \sqrt{\sum \frac{(A-nD)^2}{N}} \quad (4)$$

where A is $PL^{CI}(f,d) - FSPL(f,d_o)$ in dB, D is $10log_{10}(d)$, and N is the number of measured PL data points. The CI PLM uses a physically based reference distance d_o, and n is the mean PLE, which indicates how rapidly the PL increases with distance.

An extension of the basic CI PLM for the special case of cross-polarization is to add a constant attenuation factor, known as the cross-polarized discriminator (XPD). The CIX PLM equation is given by [16]:

$$PL^{CIX}(f,d)[dB] = FSPL(f,d_o)[dB] + 10n_{(V-V)}log_{10}(d) + XPD\ [dB] + X_\sigma^{CIX} \quad (5)$$

$$XPD = \frac{\sum A}{N} - \frac{\sum DA \sum D}{N\sum D^2} \quad (6)$$

Using the same notation as that used for the CI PLM, the zero mean Gaussian random variable is given by [14, 16, 17]:

$$X_\sigma^{CIX} = A - n_{(V-V)}D - XPD \quad (7)$$

and the standard deviation σ^{CIX} is [16, 17]:

$$\sigma^{CIX} = \sqrt{\sum \frac{X_\sigma^{CIX^2}}{N}} = \sqrt{\sum \frac{\left(A-n_{(V-V)}D-XPD\right)^2}{N}} \quad (8)$$

The FI PLM is currently used in standard work, such as the 3rd generation partnership project, and can be calculated as follows [18]:

$$PL^{FI}(d)[dB] = \alpha + 10\beta log_{10}d + X_\sigma^{FI} \quad (9)$$

Assuming B is $PL^{FI}(d)$ in dB then the zero mean Gaussian random variable is [16]:

$$X_\sigma^{FI} = B - \alpha - \beta D \quad (10)$$

and the standard deviation σ^{FI} is [16]:

$$\sigma^{FI} = \sqrt{\sum \frac{X_\sigma^{FI^2}}{N}} = \sqrt{\sum \frac{(B-\alpha-\beta D)^2}{N}} \quad (11)$$

where α is the floating intercept given by [16]:

$$\alpha = \frac{\sum D \sum BD - \sum D^2 \sum B}{(\sum D)^2 - N\sum D^2} \quad (12)$$

and β is the slope of the line (not the same as the PLE) and given by [16]:

$$\beta = \frac{\sum D \sum B - N\sum DB}{(\sum D)^2 - N\sum D^2} \quad (13)$$

where X_σ^{FI} is a lognormal random variable with 0 dB mean and standard deviation σ^{FI}.

SIMULATION SETUP USING "WIRELESS INSITE"

"Wireless InSite" is the software tool used to give the closest scenario for signals propagating from TX to RX inside the area of interest [19-20].

The area of interest (31x41x3 m) is the 4th floor inside the Faculty of Engineering at AL-Ahliyya Amman University. The floor environment consists of office partitions, meeting rooms, classrooms, and laboratories. The materials used inside the area of interest are glass, wood, concrete, metal, and different types of walls, such as brick or dry-wall, as shown in Figure 1. Two types of antenna have been used (directional and Omnidirectional) to calculate PL for co- and cross-polarized antennas at 61.5 GHz frequency.

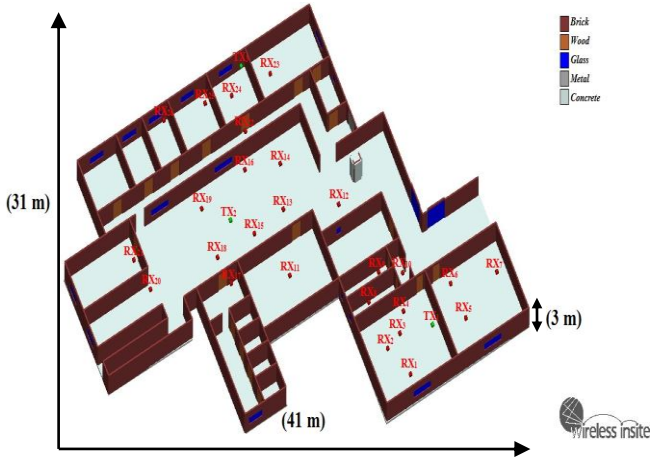

(a) Brick wall.

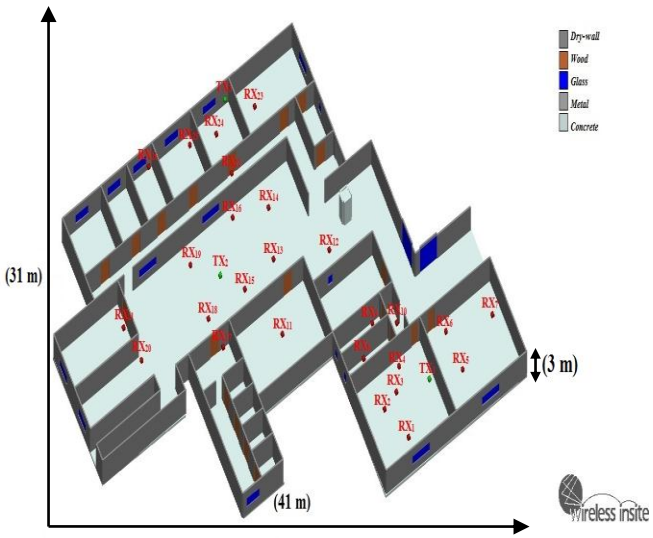

(b) Dry-wall.

Figure 1: Map of the 4th floor inside the Faculty of Engineering at AL-Ahliyya Amman University with 3 TX locations (green) and 26 RX locations (red).

Omnidirectional antennas from the PASTERNAK Company (PE-W15A001) operating between 58 to 63 GHz has been used for the TXs. Three TXs (TX_1, TX_2, and TX_3), each with 25 dBm power, 3 dBi gain, and E-plane Half-Power Beam Width (HPBW) 360°, have been employed [21]. Directional antennas from the PERASO Company (PRS1125) operating between 57 to 66 GHz were used for the RXs. A set of 26 RXs, each with 8.5 dBi gain, 90° HPBW, and threshold -80 dBm have been employed to achieve a minimum data transfer speed of 385 Mb/s [11, 22]. The electrical parameters of the materials used to build the 4th floor are presented in Table 1 [19].

Table 1: Electrical parameters used for area of interest [19]

The User Interface	Material		Relative Electrical Permittivity, ε_r	Conductivity, σ (S/m)	Thickness, (m)
Ceiling & Floor	*Concrete*		7	0.015	0.3
Walls	*Brick*		4.44	0.001	0.125
	Dry-wall	*Layer 1*	2.8	0.001	0.0130
		Layer 2	1	0.00	0.0890
		Layer 3	2.8	0.001	0.0130
Doors	*Wood*		5	0	0.03
Windows	*Glass*		2.4	0	0.003

The TX-RX separation distances range from 2.5 to 11.5 m. The TX antennas are set at height of 2 m above the floor, and the RX antennas are set at height of 1.5 m to emulate a human body. The simulation contains two antenna polarization combinations: Vertical-to-Vertical (V-V) and Vertical-to-Horizontal (V-H). The TXs are always vertically polarized, while the RXs are vertically, and then horizontally polarized.

RESULTS

Omnidirectional (for the TXs) and directional (for the RXs) antennas are used in the modeling system to calculate the parameters of the PLMs (CI, CIX, and FI) for co- and cross-polarized antennas at a 61.5 GHz frequency using the equations discussed in Section 2. Different wall materials have been used (brick and dry-wall) to show their effects on PLMs parameters.

A. Brick Wall

This study has the following limitations: TX_1 matches with the nearest RXs inside the area of interest, which number nearly 10. The TX-RX separation distance ranges from 3.3 to 8 m, as shown in Figure 2(a). TX_2 matches with 11 RXs. The TX-RX separation distance ranges from 2.7 to 11.5 m, as shown in Figure 2(b). Finally, TX_3 matches with five RXs, and the TX-RX separation distance ranges from 2.2 to 9 m, as shown in Figure 2(c).

For the V-V Line-Of-Sight (LOS) case, one PL value has been noticed for each RX that has no obstacle between itself and the TX. In the V-V NLOS case, each RX in the set has registered approximately 5 to 7 readings, based on the sensitivity of the RX. The same process was followed for the V-H LOS and NLOS cases.

For the brick wall scenario, the results have been divided into three sections. Each TX has separated parameters calculations for the CI, CIX, and FI PLMs, as shown in Figure 2.

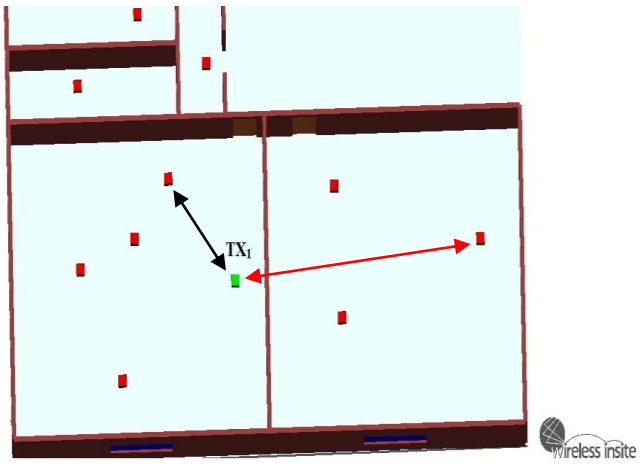

(a) Distribution of RXs around TX_1. The two arrows represent the nearest and the farthest distance between TX_1 and its RXs set.

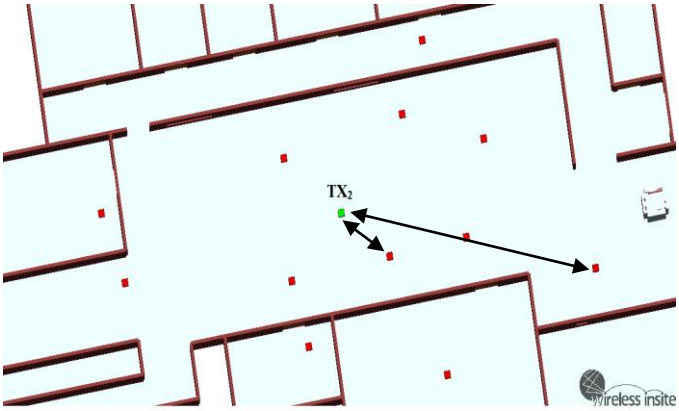

(b) Distribution of RXs around TX_2. The two arrows represent the nearest and the farthest distance between TX_2 and its RXs set.

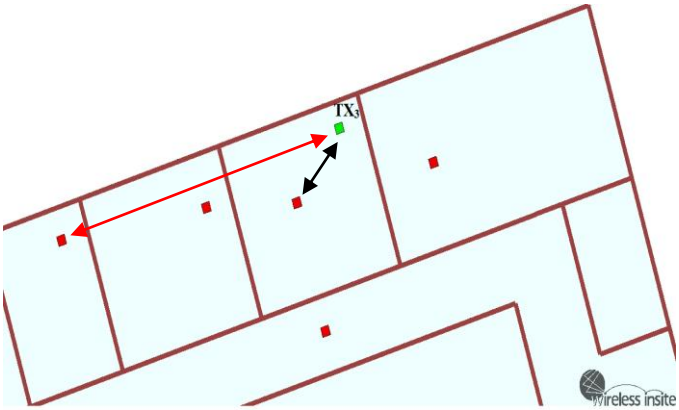

(c) Distribution of RXs around TX_3. The two arrows represent the nearest and the farthest distance between TX_3 and its RXs set.

Figure 2: Distribution of RXs around TX_1, TX_2, and TX_3. Black arrow represents LOS path and red arrow represents NLOS path.

B. TX1

Figure 3 shows the scatter plot for the CI PLM parameters for an indoor environment with co-polarized antennas at TX_1, 4 LOS and 55 NLOS readings. Figure 4 represents cross-polarized antennas case with 4 LOS and 42 NLOS readings. Table 2 summarizes the CI PLM parameters for both figures for TX_1 with $d_o = 1$ m. For TX_1, the LOS PLE for co-polarized is 1.77, which is less than the theoretical free space PLE of 2 due to waveguide effects and constructive interference from walls, the ceiling, and the floor. The Shadow Fadings (SFs) for V-V and V-H are 1.5 and 5 dB, respectively. In NLOS the SFs are 8 and 9 dB, respectively, which indicates larger fluctuation in received signal power about the mean received signal strength. The NLOS has a PLE of 4.24 for the co-polarized case due to obstructions, which require high penetration loss, and the small wavelength for the 61.5 GHz frequency. By using the strongest NLOS received power path from TX to RX (NLOS-Best), the PLE is reduced to 2.97, which is an important improvement.

Table 2: Single-frequency CI PLM with $d_o = 1$ m for TX_1

Freq.	Pol.	LOS		NLOS		NLOS-Best	
		PLE	σ^{CI} *[dB]*	*PLE*	σ^{CI} *[dB]*	*PLE*	σ^{CI} *[dB]*
61.5 GHz	V-V	1.77	1.53	4.24	8	2.97	5.833
	V-H	4.8	5	6	9	5	6.5

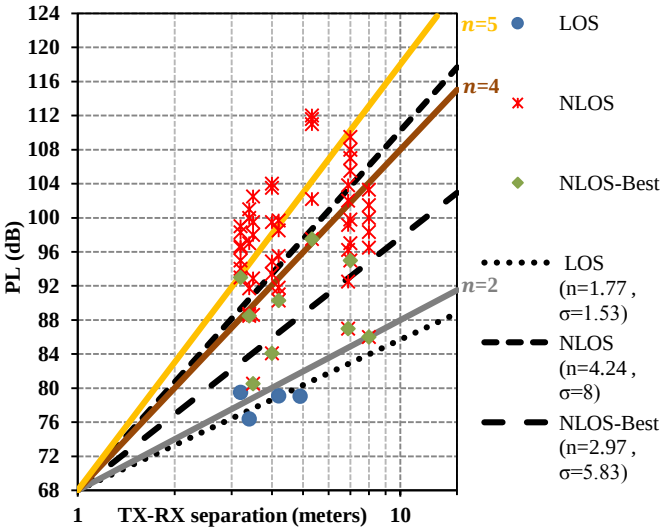

Figure 3: Single-frequency 61.5 GHz CI ($d_o = 1$ m) PLM parameters scatter plot with TX_1 at a height of 2 m, and RX antennas at a height of 1.5 m in an atypical indoor office environment for co-polarized antennas.

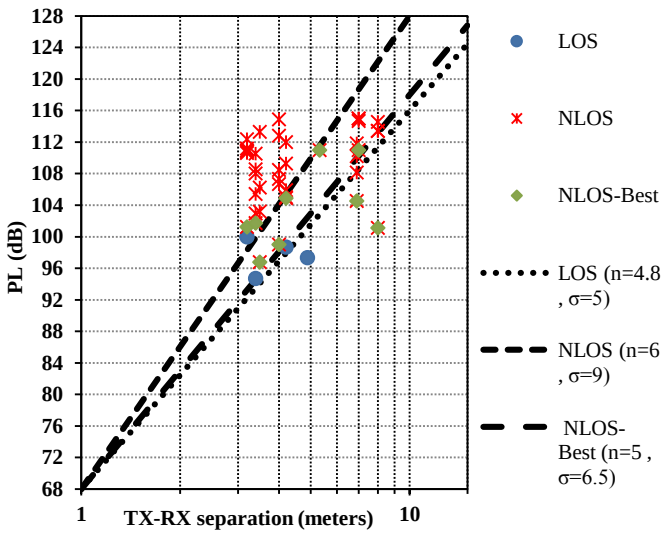

Figure 4: Single-frequency 61.5 GHz CI ($d_o = 1$m) PLM parameters scatter plot with TX_1 at a height of 2 m, and RX antennas at a height of 1.5 m in an atypical indoor office environment for cross-polarized antennas.

Table 3 displays the 61.5 GHz frequency CIX PLM parameters indoor environment for cross-polarized antennas with $d_o = 1$ m. In the CIX PLM, the same value of PLE found for the V-V co-polarized antennas has been used, and the value of XPD has been calculated using Eqn. (6). As shown in Eqn. (5), the XPD used in the CIX PLM has been added to the CI PLM to reduce the error between the simulation for cross-polarized PL and the estimator.

When examining Table 3, in the LOS case, the XPD factor is larger than that in the NLOS case by approximately 7 dB, which indicates that, in the LOS environment, the effect of the cross-polarized antennas is great. In Table 2, the LOS PLE for V-V polarization is 1.77, which is much smaller than the V-H LOS PLE of 4.88. In the NLOS case, PLEs are 4.24 and 6 for the V-V and V-H polarizations, respectively, which indicates an important depolarization effect in the NLOS indoor environment at a 61.5 GHz frequency.

The V-H CIX PLM is an efficient estimator compared to the V-H CI PLM because it has a smaller SF value (5 dB, 2.5 dB in LOS; and 9 dB, 6.5 dB in NLOS).

Table 4 shows the FI PLM parameters, NLOS and NLOS-Best, for TX_1. Here, α is the floating intercept in dB (not the same value as Free Space Path Loss (FSPL)) and β is the slope of line (not the same value as the PLE), X_σ^{FI} is a zero mean Gaussian describe signal fluctuations about the mean of PL that is like to CIX and CI PLMs. For NLOS V-V and V-H polarization cases, β values are less than PLE at same environments. This indicates a channel with extremely low loss. At TX_1, FI PLM parameters lack of fundamental physical sense.

C. TX₂

TX_2 was placed in the center of an open area along the corridor, as shown in Figure 2(b). Most RXs, located around TX_2, were in LOS with TX_2. On average, the distances between TX_2 and its RXs were the longest compared with the other sets. As a result, the travelled path distance will be the longest in this case.

Figure 5 shows the CI PLM parameters scatter plot for co-polarized antennas in an indoor environment, with 8 LOS and 58 NLOS readings. Figure 6 shows the cross-polarized antennas case, this time with 8 LOS and 25 NLOS readings. Table 5 summarizes the CI PLM parameters for both figures for TX_2 with $d_o = 1$ m. For TX_2, the LOS PLE for the co-polarized antennas is 1.8, which is larger than the LOS PLE for TX_1 due to the larger average distance between TX_2 and its RXs set. In the LOS case, the SFs for the V-V and V-H polarizations are 1.5 and 8 dB, respectively. In the NLOS case, the SFs are 10.5 and 13 dB, respectively, which indicates larger fluctuation in received signal power about the mean received signal strength. For TX_2, the NLOS PLE for the co-polarized case is 4.5, which is larger than that for TX_1. The NLOS-Best PLE is reduced to 3.33.

Table 6 summarizes the CIX PLM parameters for cross-polarized antennas. It shows that the XPD factor for the LOS case (21 dB) is larger than in the NLOS case (14 dB), while both are larger than the XPD values for TX_1. The SF in the LOS case is 1.8 and 10 dB in the NLOS case. This indicates an efficient estimator in CIX PLM compared to CI PLM.

Table 3: Single-frequency CIX PLM parameters with $d_o = 1$ m for TX_1

Freq.	Pol.	LOS			NLOS			NLOS-Best		
		$n_{(V-V)}$	XPD [dB]	σ^{CIX} [dB]	$n_{(V-V)}$	XPD [dB]	σ^{CIX} [dB]	$n_{(V-V)}$	XPD [dB]	σ^{CIX} [dB]
61.5 GHz	**V-H**	1.77	20	2.5	4.24	13	6.5	2.97	15.3	4.5

Table 4: Single-frequency FI PLM parameters for TX_1

Freq.	Pol.	NLOS			NLOS-Best		
		α [dB]	β	σ^{FI} [dB]	α [dB]	β	σ^{FI} [dB]
61.5 GHz	**V-V**	87.67	1.47	6.5	84.64	0.7	5
	V-H	101.1	1.2	4.5	92.22	1.65	4

Table 5: Single-frequency CI PLM parameters with $d_o = 1$ m for TX_2

Freq.	Pol.	LOS		NLOS		NLOS-Best	
		PLE	σ^{CI} [dB]	PLE	σ^{CI} [dB]	PLE	σ^{CI} [dB]
61.5 GHz	**V-V**	1.8	1.5	4.5	10.54	3.33	6.8
	V-H	4.52	8	5.78	13	5	10

Table 6: Single-frequency CIX PLM parameters with $d_o = 1$ m for TX_2

Freq.	Pol.	LOS			NLOS			NLOS-Best		
		$n_{(V-V)}$	XPD [dB]	σ^{CIX} [dB]	$n_{(V-V)}$	XPD [dB]	σ^{CIX} [dB]	$n_{(V-V)}$	XPD [dB]	σ^{CIX} [dB]
61.5 GHz	**V-H**	1.8	21	1.8	4.5	14	10	3.33	17	5.23

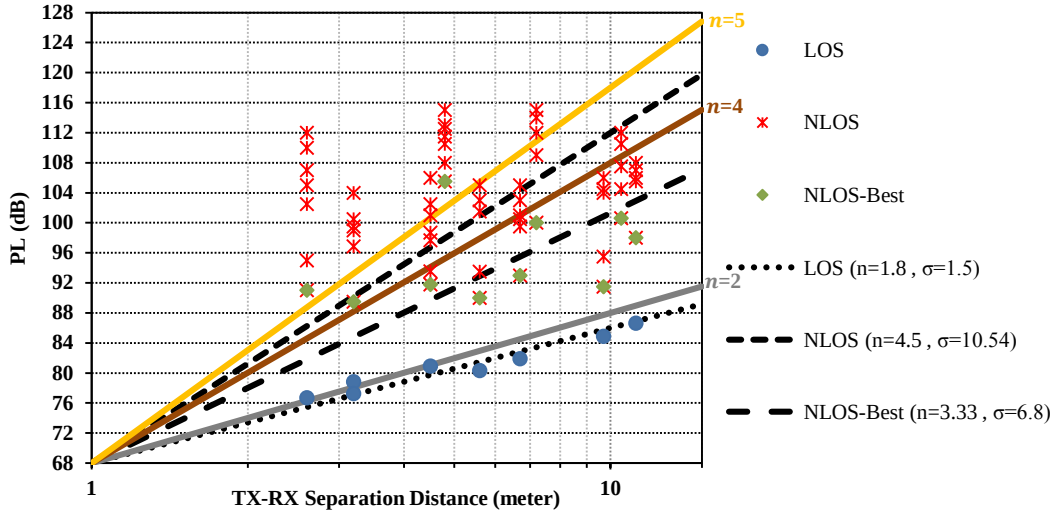

Figure 5: Single-frequency 61.5 GHz CI ($d_o = 1$ m) PLM parameters for TX_2 at a height of 2 m, and RX antennas at a height of 1.5 m in an atypical office indoor environment for co-polarized antennas.

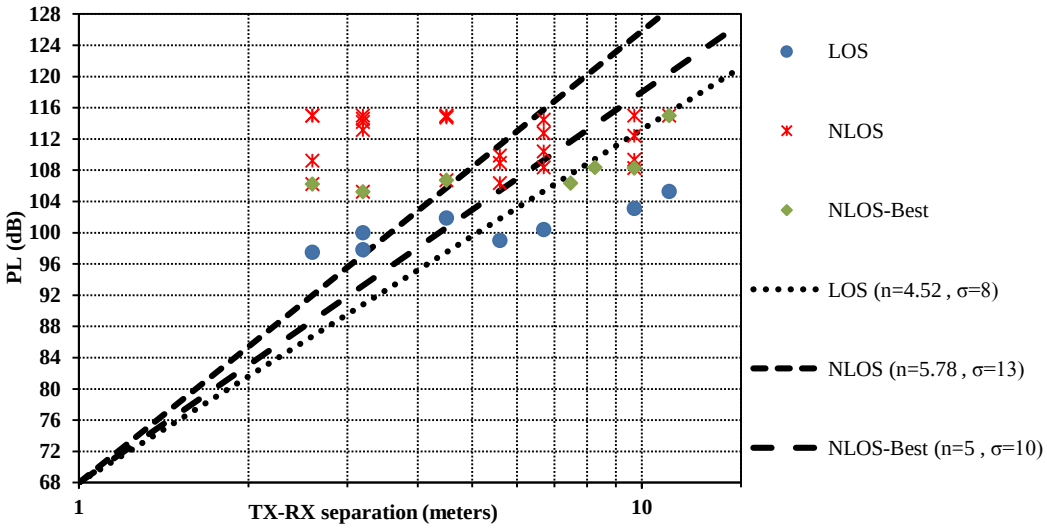

Figure 6: Single-frequency 61.5 GHz CI ($d_o = 1$ m) PLM parameters for TX_2 at a height of 2 m, and RX antennas at a height of 1.5 m in an atypical indoor office environment for cross-polarized antennas.

Table 7 shows FI PLM parameters, LOS and NLOS, for TX_2. Here, the α value for V-V polarization is larger than FSPL at 1 m in the same environment, and it is more than 20 dB compared to the V-H polarization case. This is an evidence that the FI model lacks a physical contact to the transmitted signal.

For the FI PLM at TX_1 and TX_2 in the first meters of propagation there is no physical sense of what happens in the practical NLOS or LOS scenarios, and, furthermore, the value of β ranges between 0.13 and 1.5, which is less than the PLE in the NLOS environment for both V-V and V-H polarizations. This makes it impossible to predict the fact that the NLOS V-H polarization signal is more tolerant of increased attenuation than in other cases.

Table 7: Single-frequency FI PLM parameters for TX_2

Freq.	Pol.	LOS			NLOS		
		α [dB]	β	σ^{FI} [dB]	α [dB]	β	σ^{FI} [dB]
61.5 GHz	V-V	71.2	1.45	1	99	0.54	7
	V-H	93.41	1.1	1	110.69	0.13	3.5

Since the FI model is sensitive to the data sample and the lack of a data sample, perhaps the cause of the issues with α and β isn't rooted in a physical sense. The difference in σ between the CI and FI models is small in almost all cases.

D. TX₃

TX_3 was placed in the right corner inside the second office, as shown in Figure 2(c). Most RXs, located around TX_3, were in

NLOS with TX_3. Hence, only the NLOS case was considered in this scenario. The average distances between TX_3 and its RXs were almost equal to the average distances between TX_1 and its RXs. Hence, the values of the PLM parameters in this scenario are very close to the values of the PLM parameters in the TX_1 scenario.

Figure 7 shows the scatter plot of the CI PLM parameters for co-polarized antennas in an indoor environment with 33 NLOS readings. Figure 8 depicts the cross-polarized antennas case with 25 NLOS readings. Table 8 summarizes the CI PLM parameters for both figures for TX_3 with $d_o = 1$ m. In the TX_3 scenario, the NLOS PLE for co-polarized antennas is 4, which is almost equal to the NLOS PLE for TX_1. The SFs for co- and cross-polarized antennas are 11.5 and 12.5 dB, respectively, which are the highest values of SF obtained in the three scenarios.

Table 9 summarizes CIX PLM parameters for cross-polarized antennas. The XPD value is 13.2 dB, which is similar to the XPD value (13 dB) from Table 3. The similarity between the two scenarios leads to almost similar values for the PLMs parameters, which confirms their validity.

Table 8: Single-frequency CI PLM parameters with $d_o = 1$ m for TX_3

Freq.	Pol.	NLOS		NLOS-Best	
		PLE	σ^{CI} *[dB]*	*PLE*	σ^{CI} *[dB]*
61.5 GHz	V-V	4	11.5	2.92	10.59
	V-H	5.6	12.5	5	14.2

Table 9: Single-frequency CIX PLM parameters with $d_o = 1$ m for TX_3

Freq.	Pol.	NLOS			NLOS-Best		
		$n_{(V-V)}$	*XPD [dB]*	σ^{CIX} *[dB]*	$n_{(V-V)}$	*XPD [dB]*	σ^{CIX} *[dB]*
61.5 GHz	V-H	4	13.2	10	2.92	17	9.8

E. Dry-wall

In this section, the material of the wall has been switched from brick to dry-wall. The same simulation procedures in the previous section have been followed to discover the impact of changing material on the values of PL parameters, as depicted in Figure 1(b). For indoor propagation, it is important to study characterized power attenuation in relation to electrical parameters [23].

Table 1 shows that the materials, brick and dry-wall, have a small difference in thickness, but the value of ε_r in the brick material (4.44) is larger than that for the dry-wall material (2.8). Tables 10, 11, and 12 summarize the CI PLM for co- and cross-polarized antennas in an indoor environment for TX_1, TX_2, and TX_3.

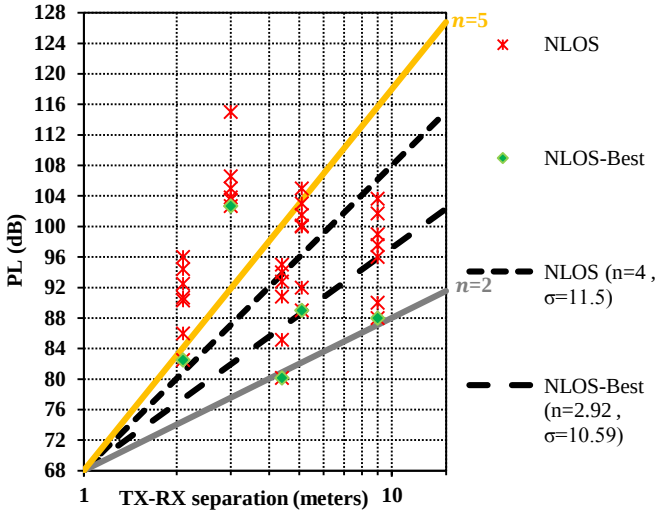

Figure. 7: Single-frequency 61.5 GHz CI ($d_o = 1$ m) PLM parameters for TX_3 at a height of 2 m, and RX antennas height of 1.5 m in an atypical indoor office environment for co-polarized antennas.

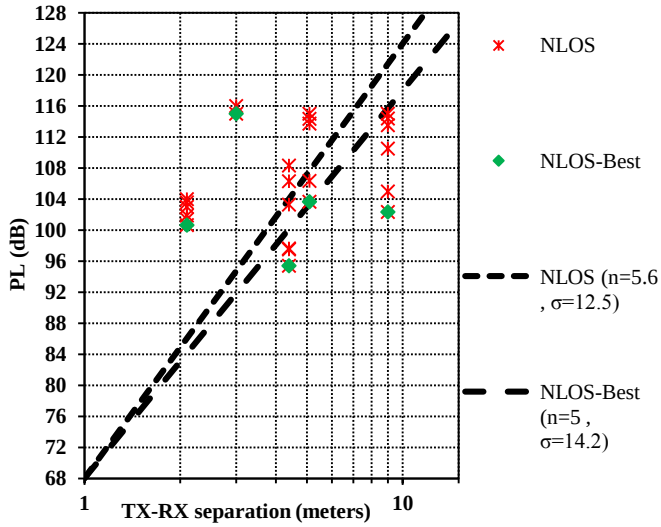

Figure. 8: Single-frequency 61.5 GHz CI ($d_o = 1$ m) PLM parameters for TX_3 at a height of 2 m, and RX antennas height of 1.5 m in an atypical indoor office environment for cross-polarized antennas.

Table 10 summarizes the dry-wall scenario for TX_1. The NLOS PLE for the co-polarized antenna is 4.19, which is less than the PLE for the brick wall under the same conditions. For TX_2 and TX_3, Tables 11 and 12 show that the values of PLE for co-polarized antennas are also less for the dry-wall than brick wall under the same conditions. These values are 4.33 and 4.13, respectively. The values of the SF are almost identical for the two scenarios. For the dry-wall scenario, Tables 13, 14, and 15 summarize the parameters for the CIX PLM with cross-polarized antennas in an indoor environment for TX_1, TX_2, and TX_3, respectively.

Table 10: Single-frequency CI PLM parameters with $d_o = 1$ m for TX_1

Freq.	Pol.	LOS		NLOS		NLOS-Best	
		PLE	***σ^{CI} [dB]***	***PLE***	***σ^{CI} [dB]***	***PLE***	***σ^{CI} [dB]***
61.5 GHz	**V-V**	1.77	1.53	4.19	7	2.29	5.97
	V-H	4.8	5	5.8	8	5	7.24

Table 11: Single-frequency CI PLM parameters with $d_o = 1$ m for TX_2

Freq.	Pol.	LOS		NLOS		NLOS-Best	
		PLE	***σ^{CI} [dB]***	***PLE***	***σ^{CI} [dB]***	***PLE***	***σ^{CI} [dB]***
61.5 GHz	**V-V**	1.8	1.5	4.33	8.52	3.5	7.2
	V-H	4.52	8	6	11.5	5.4	10

Table 12: Single-frequency CI PLM parameters with $d_o = 1$ m for TX_3

Freq.	Pol.	NLOS		NLOS-Best	
		PLE	***σ^{CI} [dB]***	***PLE***	***σ^{CI} [dB]***
61.5 GHz	**V-V**	4.13	11.22	2.92	8.87
	V-H	5.3	12	4.39	9

Table 13: Single-frequency CIX PLM parameters with $d_o = 1$ m for TX_1

Freq.	Pol.	LOS			NLOS			NLOS-Best		
		$n_{(V-V)}$	***XPD[dB]***	***σ^{CIX} [dB]***	***$n_{(V-V)}$***	***XPD [dB]***	***σ^{CIX} [dB]***	***$n_{(V-V)}$***	***XPD [dB]***	***σ^{CIX} [dB]***
61.5 GHz	**V-H**	1.77	20	2.5	4.19	12.3	6	2.29	16	5.14

Table 14: Single-frequency CIX PLM parameters with $d_o = 1$ m for TX_2

Freq.	Pol.	LOS			NLOS			NLOS-Best		
		$n_{(V-V)}$	***XPD [dB]***	***σ^{CIX} [dB]***	***$n_{(V-V)}$***	***XPD [dB]***	***σ^{CIX} [dB]***	***$n_{(V-V)}$***	***XPD [dB]***	***σ^{CIX} [dB]***
61.5 GHz	**V-H**	1.8	21	1.8	4.33	14	8.5	3.5	16	6

Table 15: Single-frequency CIX PLM parameters with $d_o = 1$ m for TX_3

Freq.	Pol.	NLOS			NLOS-Best		
		$n_{(V-V)}$	***XPD [dB]***	***σ^{CIX}[dB]***	***$n_{(V-V)}$***	***XPD [dB]***	***σ^{CIX}[dB]***
61.5 GHz	**V-H**	4.13	11	9	2.92	13	5.4

For the NLOS case, the XPD factors for TX_1, TX_2, and TX_3 are 12.3, 14, and 11 dB, respectively. These values are less than or equal to the brick wall material XPD values, which are 13, 14, and 13.2 dB, respectively. This shows the impact of ε_r on PLE values for the NLOS case.

DELAY SPREAD

In wireless communication system, transmitted data are received by the RX after passing through a radio channel, which can be represented by an unknown time-varying filter. Transmitted signals are scattered and reflected, reaching the RX through many paths. Images of different symbols arrive at the same time, causing Inter Symbol Interference (ISI). ISI due to time dispersion is treated with an equalization technique. Huge data rates, with narrower symbol duration, requiring highly complex process equalizers [24].

The Root Mean Square (RMS) delay spread is defined as the square root of the second central moment of the power delay profile, and the formula for calculating the RMS delay spread is defined as [13, 25, 26]:

$$\sigma_{RMS} = \sqrt{\bar{t^2} - \bar{t}^2} \tag{14}$$

RMS delay spread is explained mathematically in detail in the following equations [13]:

$$\sigma_{RMS} = \sqrt{\frac{\sum_{i=1}^{N_P} P_i t_i^2}{P_R} - \bar{t}^2} \tag{15}$$

where P_R is the average received power, N_P is the number of paths, P_i is the time averaged power in watts of the i^{th} path, and t_i is the time of arrival [13]:

$$t_i = \frac{L_i}{c} \tag{16}$$

where L_i is the total geometrical path length and c is the speed of light in free space. The mean time of arrival is [13]:

$$\bar{t} = \frac{\sum_{i=1}^{N_p} P_i t_i}{P_R} \quad (17)$$

Figures 9 and 10 display the Cumulative Distribution Function (CDF) for the RMS delay spread, with a combined two scenarios of LOS and NLOS, at a 61.5 GHz frequency for V-V and V-H polarizations, respectively. Both figures show that the RMS delay spread is less than 30 ns for both scenarios in an indoor environment at a 61.5 GHz frequency. The means of the RMS delay spreads are between 8 to 20 ns. These values are within acceptable range for a 60 GHz band [27].

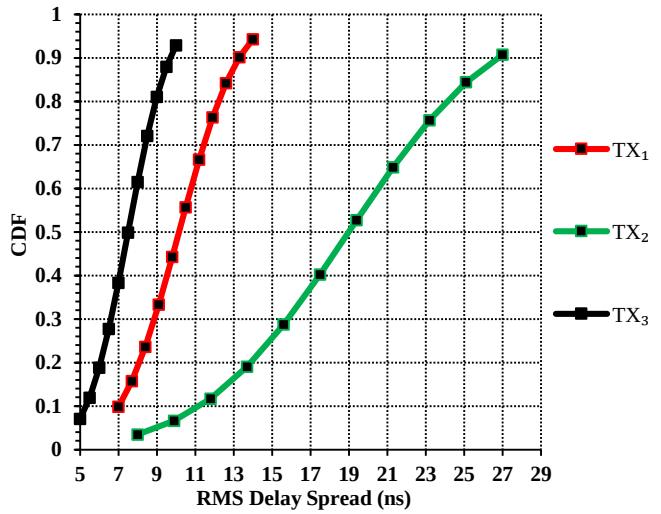

Figure 9: A CDF plot showing the RMS delay spread for V-V polarization case.

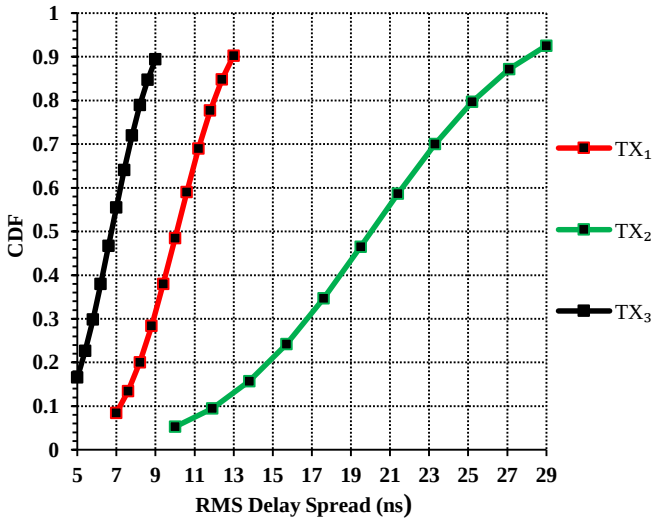

Figure 10: A CDF plot showing the RMS delay spread for V-H polarization case.

The mean RMS delay spread at 61.5 GHz is larger than the mean RMS at 73 GHz (8 to 13 ns) and lower than the mean RMS at 2.25 GHz by approximately 40%(20 to 28 ns) due to high penetration caused by walls. At 61.5 GHz, multipath components have been observed that came from reflected waves in the same room, but, at 2.25 GHz, the reflected waves came from neighboring rooms, and had a significantly longer delay [16].

At TX_2, the mean RMS delay spread is 20 ns which is the largest value for the TXs in both the LOS and NLOS cases. Actually, the mean RMS delay spread in the NLOS case is larger than in the LOS case at the same location since obstructions attenuated or blocked the direct path, causing multipaths to reach the RXs over a larger time interval, and making the travel distances longer. Moreover, paths need a longer propagation time interval to reach the RXs from TX_2, because the travel distances are greater than they are for TX_1 and TX_3.

At 61.5 GHz, the RMS delay spread for V-H polarization is larger than that for V-V polarization, most likely due to the capture of extra energy in an indoor mm-wave environment (based on wave cross-polarized antennas from TX to RX). In addition, in some cases like TX_2, a larger RMS delay spread (1 to 2 ns) has been noticed for V-H polarization compared to V-V polarization [16].

CONCLUSION

This research provided a study of an indoor mm-wave channel at 61.5 GHz frequency. Using different types of antennas, polarizations, and materials, an RMS delay spread and PLM (CI, CIX, and FI) parameters were generated.

Analysis showed that, for the 61.5 GHz indoor environment scenarios, the large-scale PL over distance was modeled with good precision and required just one parameter for the CI PLM to insure a physical tie to the TX power. The FI PLM lacked intuition and required an additional parameter.

The CI PLM for co-polarized antennas as appeared to have a constructive interference due to wave guiding and reflections. This resulted in nearly identical LOS PLEs of 1.77 and 1.8 for TX_1 and TX_2, respectively, both smaller than the theoretical FSPL PLE (n=2).

In the NLOS case, the PL suffered greater attenuation than in the LOS case. This amounted to 42.4 dB (n=4.24), 45 dB (n=4.5), and 40 dB (n=4) per decade of distance for TX_1, TX_2, and TX_3, respectively. Using the same scenarios, the large attenuations were significantly reduced (resulting in n=2.97 for TX_1, n=3.33 for TX_2, and n=2.92 for TX_3) when NLOS-Best was used. The SF increased from LOS to NLOS for all RXs, which indicated a large signal fluctuation in the NLOS case.

The PLE for cross-polarized antennas indicated significant depolarization in the NLOS indoor environment at 61.5 GHz. For the LOS case, the largest XPD factors of 20 and 21 dB

were found for cross-polarized antennas in TX_1 and TX_2, respectively. In the CIX PLM, there was less fluctuation in received signal strength about the mean compared to the CI cross-polarized antennas PLM. The CIX is a simple and useful PLM for cross-polarized antennas systems, and it improved the SF when compared to CI PLM. The CIX SF was reduced by 2.5 dB for both cases, LOS and NLOS, at TX_1. For TX_2, the SF was reduced by 6.2 and 3 dB for LOS and NLOS, respectively.

The FI PLM lacked a physical basis for electromagnetic propagation. The CI PLM explained better the physical propagation at 61.5 GHz compared to FI PLM. In the TX_2 scenario, the values of β for V-V polarization were 1.45 and 0.54 for LOS and NLOS cases, respectively. This indicates no meaning for PL with distance using the FI PLM. The better stability and physical sensibility of CI PLM was due to the fixation of received power at 1 m from the TX. The FI PLM required two parameters, while the CI PLM required just one parameter.

At TX_2, the LOS PLE for co-polarized antennas was 1.8, which was larger than the PLE for TX_1, and due to the larger distance between TX_2 and its RXs. Also, in the V-V NLOS case, the value of the PLE was larger than it was in the TX_1 scenario. The difference in σ between the two TXs was small in almost all cases.

In Section 4 (E), the material of walls has changed from brick to dry-wall and the value of ε_r decreased from 4.44 to 2.8. Hence, the value of PL also decreased. For dry-wall scenario, the NLOS PLE for V-V polarization was less than the value for the brick walls scenario. Using the NLOS-Best at TX_1, the value of PLE decreased from 2.97 to 2.29, but the SF was equal in all cases.

Ninety-percent of RMS delay spread was under 28 ns for both LOS and NLOS environments. The mean RMS delay spread for the three TXs was between 6 to 19 ns for V-V polarization and 6 to 20 ns for V-H polarization. The reasons behind the difference in values of the mean RMS delay spread between the three TXs are related to the different distances, in total, between each TX and its RXs, and the number of obstacles that the paths faced.

REFERENCES

[1] Sun, Shu, Theodore S. Rappaport, Sundeep Rangan, Timothy A. Thomas, Amitava Ghosh, Istvan Z. Kovacs, Ignacio Rodriguez, Ozge Koymen, Andrzej Partyka, and Jan Jarvelainen. "Propagation path loss models for 5G urban micro-and macro-cellular scenarios." In Vehicular Technology Conference (VTC Spring), 2016 IEEE 83rd, pp. 1-6. IEEE, 2016.

[2] Dheyab, Ehab, and Nidal Qasem. "Design and Optimization of Rectangular Microstrip Patch Array Antenna Using Frequency Selective Surfaces for 60 GHz." International Journal of Applied Engineering Research 11, no. 7 (2016): 4679-4687.

[3] Pi, Zhouyue, and Farooq Khan. "An introduction to millimeter-wave mobile broadband systems." IEEE Communications Magazine 49, no. 6 (2011).

[4] Rappaport, Theodore S., Shu Sun, Rimma Mayzus, Hang Zhao, Yaniv Azar, Kevin Wang, George N. Wong, Jocelyn K. Schulz, Mathew Samimi, and Felix Gutierrez. "Millimeter wave mobile communications for 5G cellular: It will work!." IEEE access 1 (2013): 335-349.

[5] Rappaport, Theodore S., George R. MacCartney, Mathew K. Samimi, and Shu Sun. "Wideband millimeter-wave propagation measurements and channel models for future wireless communication system design." IEEE Transactions on Communications 63, no. 9 (2015): 3029-3056.

[6] Niu, Young, Youg Li, Depeng Jin, Li Su, and Athanasios V. Vasilakos. "A Survey of Millimeter Wave (mmWave) Communications for 5G: Opportunitios and Challenges." Computer Science-Networking and Internet Architecture (2015).

[7] Haneda, Katsuyuki, Jianhua Zhang, Lei Tan, Guangyi Liu, Yi Zheng, Henrik Asplund, Jian Li et al. "5G 3GPP-like channel models for outdoor urban microcellular and macrocellular environments." In Vehicular Technology Conference (VTC Spring), 2016 IEEE 83rd, pp. 1-7. IEEE, 2016.

[8] Verma, Lochan, Mohammad Fakharzadeh, and Sunghyun Choi. "Wifi on steroids: 802.11 ac and 802.11 ad." IEEE Wireless Communications 20, no. 6 (2013): 30-35.

[9] Alkhawatra, Mohammad, and Nidal Qasem. "Improving and Extending Indoor Connectivity Using Relay Nodes for 60 GHz Applications." INTERNATIONAL JOURNAL OF ADVANCED COMPUTER SCIENCE AND APPLICATIONS 7, no. 4 (2016): 427-434.

[10] De Alwis, Gayan, and Murray Delahoy. "MILLIMETRE WAVE TECHNOLOGY."

[11] Daniels, Robert C., James N. Murdock, Theodore S. Rappaport, and Robert W. Heath. "60 GHz wireless: Up close and personal." IEEE Microwave Magazine 11, no. 7 (2010): 44-50.

[12] Ghaddar, Mohamad, Larbi Talbi, Gilles Y. Delisle, and Jules LeBel. "Deflecting-obstacle effects on signal propagation in the 60 GHz band." IEEE Transactions on antennas and propagation 61, no. 1 (2013): 403-414.

[13] Qasem, Nidal, Emran Ali Aldorgam, and Hadeel Yaseen Alzou'bi. "Overcoming the Influence of Human Shadowing and Obstacles via Modified Building Using

Frequency Selective Wallpapers for 60 GHz." Journal of Communication and Computer 13 (2016): 90-101.

[14] MacCartney, George R., Sijia Deng, and Theodore S. Rappaport. "Indoor office plan environment and layout-based mmWave path loss models for 28 GHz and 73 GHz." In Vehicular Technology Conference (VTC Spring), 2016 IEEE 83rd, pp. 1-6. IEEE, 2016.

[15] Daniels, Robert C., and Robert W. Heath Jr. "60 GHz wireless communications: Emerging requirements and design recommendations." IEEE Vehicular Technology Magazine 2, no. 3 (2007).

[16] Maccartney, George R., Theodore S. Rappaport, Shu Sun, and Sijia Deng. "Indoor office wideband millimeter-wave propagation measurements and channel models at 28 and 73 GHz for ultra-dense 5G wireless networks." IEEE Access 3 (2015): 2388-2424.

[17] Feuerstein, Martin J., Kenneth L. Blackard, Theodore S. Rappaport, Scott Y. Seidel, and Howard H. Xia. "Path loss, delay spread, and outage models as functions of antenna height for microcellular system design." IEEE Transactions on Vehicular Technology 43, no. 3 (1994): 487-498.

[18] MacCartney, George R., Mathew K. Samimi, and Theodore S. Rappaport. "Omnidirectional path loss models in New York City at 28 GHz and 73 GHz." In Personal, Indoor, and Mobile Radio Communication (PIMRC), 2014 IEEE 25th Annual International Symposium on, pp. 227-231. IEEE, 2014.

[19] "Wireless EM Propagation Software - Wireless InSite." Remcom [Online]. Available: https://www.remcom.com/wireless-insite-em-propagation-software. [Accessed: 31-Oct-2017].

[20] Qasem, Nidal. "Enhancing wireless communication system performance through modified indoor environments." PhD diss., © Nidal Qasem, 2014.

[21] "WR-15 Waveguide Horn Antenna Operating From 58 GHz to 63 GHz With a Nominal 0 dBi Gain." Pasternack. [Online]. Available: https://www.pasternack.com/omnidirectional-antenna-58-63-ghz-0-dbi-gain-wr-15-waveguide-pe-w15a001-p.aspx. [Accessed: 31-Oct-2017].

[22] "PRS4000/PRS1025 60 GHz WiGig Chipset." Perasotech. [Online]. Available: http://www.perasotech.com/wp-content/uploads/2015/03/prs4000_1025-product_brief-rev0-15-03.pdf. [Accessed: 31-Oct-2017].

[23] Qureshi, Umair Mujtaba, Faisal Karim Shaikh, Zuneera Aziz, Syed M. Zafi S. Shah, Adil A. Sheikh, Emad Felemban, and Saad Bin Qaisar. "Rf path and absorption loss estimation for underwater wireless sensor networks in different water environments." Sensors 16, no. 6 (2016): 890.

[24] Arslan, Hüseyin, and Tevfik Yucek. "Delay spread estimation for wireless communication systems." In Computers and Communication, 2003.(ISCC 2003). Proceedings. Eighth IEEE International Symposium on, pp. 282-287. IEEE, 2003.

[25] Hassan, K., T. A. Rahman, M. R. Kamarudin, and F. Nor. "The mathematical relationship between maximum access delay and the RMS delay spread." In The Seventh International Conference on Wireless and Mobile Communications (ICWMC 2011), Luxembourg, pp. 18-23. 2011.

[26] Qasem, Nidal, and Rob Seager. "Parametric studies in enhancing indoor wireless communication system via environmental modification." In Antennas and Propagation Conference (LAPC), 2012 Loughborough, pp. 1-4. IEEE, 2012.

[27] Rappaport, Theodore S., Eshar Ben-Dor, James N. Murdock, and Yijun Qiao. "38 GHz and 60 GHz angle-dependent propagation for cellular & peer-to-peer wireless communications." In Communications (ICC), 2012 IEEE International Conference on, pp. 4568-4573. IEEE, 2012.